NASA CONTRACTOR REPORT 187626

Interior Noise Prediction Methodology: ATDAC Theory and Validation

Gopal P. Mathur and Bryce K. Gardner

DOUGLAS AIRCRAFT COMPANY
MCDONNELL DOUGLAS CORPORATION
LONG BEACH, CA 90846

CONTRACT NAS1-18037
APRIL 1992

National Aeronautics and
Space Administration

Langley Research Center
Hampton, Virginia 23665-5225

Preface

This report was prepared by McDonnell Douglas Corporation under Task Assignment 7 of Contract NAS1-18037 with NASA Langley Research Center. The NASA technical monitor was Dr. Kevin P. Shepherd.

Several individuals at Douglas Aircraft Company have made major contributions to this study. The second author, Bryce Gardner, made significant contributions towards ATDAC theoretical modelling in the initial phase of this task. The computer coding of the ATDAC program was done by John Winfrey, Mark Cannon and Boi Tran. Special thanks go to Myles Simpson and Dr. Mahendra Joshi for reviewing the report and providing many constructive comments throughout this task.

Contents

List of Figures

1 Introduction

The Acoustical Theory for Design of Aircraft Cabins (ATDAC) is a computer program developed to predict interior noise levels inside aircraft and to evaluate the effects of different aircraft configurations on the aircraft acoustical environment. The primary motivation for development of this program is the special interior noise problems associated with advanced turbo-prop (ATP) aircraft where there is a tonal, low frequency noise problem. This report describes the theory and equations implemented in the ATDAC program. A description of the program structure and the operating instructions is contained in the user's manual: "Interior Noise Prediction Methodology–ATDAC User's Manual." [1]

Prediction of interior noise levels requires knowledge of the energy sources, the transmission paths, e.g., structural elements and the relationship between the energy variable and the sound pressure level. The energy sources include engine noise, both airborne and structure-borne; turbulent boundary layer noise; and interior noise sources such as air conditioner noise and auxiliary power unit noise. Since propeller and engine noise prediction programs are widely available, they are not included in ATDAC. Airborne engine noise from any prediction or measurement may be input to this program. ATDAC includes modules which predict the contribution of boundary layer noise and structure-borne noise from the engine. Several ways of predicting structure-borne noise are discussed in Section 4. The turbulent boundary layer noise algorithm is presented in Section 5. The acoustical power from the noise sources inside the aircraft may also be input to ATDAC.

The energy produced by exterior noise sources propagates to and impinges on a panel at some point. The transmission loss module predicts the energy behavior at the panel by predicting the transmission loss and reflection co-efficients of the panel. The theory to predict transmission and radiation properties is described in Section 3. The transmission loss and reflection co-efficients are put in a database of panel designs. Any experimental panel data may be included in the database.

The energy sources and panel properties are combined with a description of the aircraft's geometrical configuration to predict the interior noise levels. A geometry module defines the volumes and panels for a particular aircraft. The power balance takes the source data, the transmission and reflection data and the geometry data and solves for the net intensities into each volume. Then the interior sound pressure levels are calculated. The form of the power balance is based on the room equation and is described in the next section.

2 Energy Balance and the Room Equation

2.1 Introduction

The ATDAC noise prediction method is based on a modified form of the acoustic room equation. The acoustic room equation, in its common form, was published by Embleton [2]. The room equation has been widely used, especially in the field of architectural acoustics. Many empirical corrections have been proposed for the room equation but none will be used in this implementation so that the method will be as general purpose as possible. The room equation, however, has been modified for use in the present noise prediction methodology. The choice of using the room equation represents a compromise between accuracy and simplicity.

The accurate prediction of sound contained in a multiply-connected system of enclosures is a difficult problem involving the knowledge of both the structural and the acoustic behavior and how they interact. For a system of any size at any frequency range but the lowest, the set of equations resulting from numerically solving the wave equation in the cavity coupled with the equations of motions for the structure is very large. When the size of the system of equations is combined with the extensive modelling that must be done to generate those equations, it is prohibitively expensive to analyze most realistic structural/acoustic systems utilizing first principles. This is especially true when multiple trade studies must be done to evaluate many alternatives. By using the room equation, the sound pressure levels in large structural/acoustic systems can be evaluated quickly. Because the room equation uses an energy or power balance formulation, the structural equations are decoupled from the acoustical equations and therefore detailed analysis may be done on specific portions of the model and later the results can be substituted into the overall prediction. In the same way, experimental results for specific components may be used.

2.2 Assumptions

In order to use any theory well, the assumptions and limitations must be understood. This is particularly important in this case because the simplicity of its use may lead to trying to draw more conclusions than are appropriate.

These assumptions are as follows:

- the system has reached steady state conditions.
- the sound field in the room is completely diffuse and reverberant so that the sound energy density is uniform throughout the room. This implies that the absorption

is small and uniformly distributed.

- the mean free path (MFP), which is the average distance sound travels between reflections, must follow

$$MFP = \frac{4V}{S}, \tag{1}$$

where V is the room volume and S is the total surface area of all the walls. This criteria is usually met if the lengths of the sides of the room are all of the same order of magnitude.

- All noise sources are sufficiently distributed so that the direct field may be ignored.

Because the major sources are spatially distributed in aircraft, the assumption of a diffuse field is reasonable except where the response is largely dominated by one or two modes.

2.3 Derivation

In terms of engineering units, the room equation can be written

$$|p|^2 = W\rho c\left(\frac{Q_\theta}{4\pi r^2} + \frac{4}{R}\right) \tag{2}$$

where p is the acoustic pressure, W is the power generated in the room, ρ is the air density, c is the speed of sound in air, Q_θ is the directivity factor of the source, r is the distance from the source, and R is the room constant. The term $\frac{Q_\theta}{4\pi r^2}$ represents the energy in the field directly radiated by the source and the term $\frac{4}{R}$ represents the energy in the reverberant field. Splitting up the energy terms into direct and indirect fields requires detailed knowledge of the energy sources. A modified room constant can be defined in which the term describing the direct field is absorbed into the reverberant energy term giving the equation

$$|p|^2 = W\rho c\left(\frac{4}{R'}\right) \tag{3}$$

where R' is the modified room constant. After absorbing the direct field term into the reverberant field term and realizing that the intensity in a completely reverberant field is

$$I = \frac{|p|^2}{4\rho c}, \tag{4}$$

the room equation can be written as

$$R'I = W. \tag{5}$$

Because the room equation was derived for a source in a room, the input power is modified in this derivation to include all the power coming into a room. By expanding the definition of W this way, equation (5) can be rewritten

$$R'I = \sum_{k=1}^{\#ofSurfaces} W_k + \sum_{l=1}^{\#ofSources\ in\ Room} W_l, \tag{6}$$

where W_k is the power coming into the room through the kth surface and W_l is the power generated by the lth source in the room. The power coming through a surface is given by

$$W_k = IS\tau, \tag{7}$$

where I is the intensity incident on the other side of the surface, S is the area of the surface and τ is the transmission co-efficient of the surface. If the room is connected to other rooms, some with known intensities (type A) and some with unknown intensities (type B), the room equation may be rewritten as

$$R'I - \sum_{k=1}^{\#ofType\ B\ Surfaces} I_k S_k \tau_k = \sum_{m=1}^{\#ofType\ A\ Surfaces} I_m S_m \tau_m + \sum_{l=1}^{\#ofSources\ in\ Room} W_l. \tag{8}$$

On the left hand side of equation 8 all the intensities, I, are unknown but on the right hand side all the variables are known. As it is, equation 8 is ill-posed but more equations can be written. If one equation is written for each room or volume where the intensities are not known and the intensities are known outside of all exterior walls or surfaces, then a system of equations can be written in matrix form for a set of n rooms or volumes

$$\begin{bmatrix} R'_1 & S\tau_{12} & S\tau_{13} & \cdots & S\tau_{1n} \\ & R'_2 & S\tau_{23} & \cdots & S\tau_{2n} \\ & & \ddots & & \vdots \\ & (SYM.) & & & \\ & & & & R'_n \end{bmatrix} \begin{Bmatrix} I_1 \\ I_2 \\ \vdots \\ I_n \end{Bmatrix} = \begin{Bmatrix} W'_1 \\ W'_2 \\ \vdots \\ W'_n \end{Bmatrix}, \tag{9}$$

where

$$W'_i = \sum_{m=1}^{\#ofExterior\ Surfaces} I_{im} S_{im} \tau_{im} + \sum_{l=1}^{\#ofSources\ in\ Volume\ i} W_{il}$$

and

$$S\tau_{ij} = \sum_{k=1}^{\#ofSurfaces\ connecting\ Volumes\ i\&j} S_k \tau_k.$$

Every term in equation (9) has been defined except R', the modified room constant. The room constant is typically defined as [2]

$$R = \frac{S_t \bar{\alpha}}{1 - \bar{\alpha}} \tag{10}$$

where S_t is the total surface area of the boundary of the volume or room and $\bar{\alpha}$ is the average statistical absorption co-efficient. The $1 - \bar{\alpha}$ term represents the ratio of energy left after the first reflection or the ratio of the energy supplied to the reverberant field from the direct field. In order to make the room constant account for all of the energy lost from the room, the energy lost during the first reflection must be included. The modified room constant which includes all the energy is

$$R' = S_t \bar{\alpha}. \tag{11}$$

The average statistical absorption co-efficient is defined by

$$\bar{\alpha} = \frac{\sum_{k=1}^{\#of\ Boundary\ Surfaces} S_k \alpha_k}{\sum_{k=1}^{\#of\ Boundary\ Surfaces} S_k} \tag{12}$$

The statistical absorption co-efficient α is defined as the ratio of the power absorbed (Π_a) to the power incident (Π_i)

$$\alpha = \frac{\Pi_a}{\Pi_i}, \tag{13}$$

or the ratio of energy that is not reflected

$$\alpha = 1 - r. \tag{14}$$

Here r is the statistical reflection co-efficient and is defined as

$$r = \frac{\Pi_r}{\Pi_i}, \tag{15}$$

where Π_r is the power reflected.

If there are other absorbing surfaces (such as seats) which are not part of the walls of the volume, the effects of the absorption of these other surfaces can be included in the modified room constant as

$$R' = S_t \bar{\alpha} + \sum_{k=1}^{\#of\ Non-Boundary\ Surfaces} S_k \alpha_k. \tag{16}$$

If the volume is large, then the effect of absorption in the air must be added to the room constant. The air absorption term is $4mV$ where m is the energy attenuation constant and V is the room volume.

3 Transmission Loss Theory and Validation

3.1 Introduction

Transmission loss (TL) is the classical measure of the installation-independent sound insulation properties of a panel, and it is defined in terms of the transmission co-efficient τ,

$$TL = 10 \log \frac{1}{\tau}. \tag{17}$$

In the modified room equation presented in Section 2, all walls or partitions are completely characterized with transmission and reflection co-efficients, τ and r. Much work has been done to predict and measure the transmission co-efficient. The reflection co-efficient has not received nearly as much attention, but it can be derived from the same equations that are used to predict the transmission co-efficient.

The transmission loss model used in this study is based on an infinite panel theory. Although infinite panel theory does not take into account all the details of a fuselage sidewall or panel, it does predict the effects of several panel design parameters in a reasonable way [3]. The prediction of *in situ* transmission loss of a panel in its actual location in the fuselage or structure will require detailed theoretical modelling of the entire structure and installation. An infinite panel transmission loss theory, though simple in approach, will predict the effects of panel properties without detailed knowledge of the installation.

3.2 Theory

3.2.1 Definitions

The transmission co-efficient τ is defined as the ratio of the transmitted acoustic power to the incident acoustic power

$$\tau = \frac{\Pi_t}{\Pi_i}. \tag{18}$$

Similarly, the reflection co-efficient r is defined as the ratio of the reflected acoustic power to the incident acoustic power

$$r = \frac{\Pi_r}{\Pi_i}. \tag{19}$$

The absorption co-efficient is defined as the ratio of the acoustic power that is not reflected to the incident acoustic power or

$$\alpha = 1 - r. \tag{20}$$

3.2.2 Single Panel Transmission Loss

The transmission loss equations for single and double wall infinite partitions are derived in many acoustics text books [3] [4]. Since the TL equations are derived for a specific panel design, any deviation or added complexity in a panel would require a complete rederivation. The transmission loss equations for a single, infinite panel are given in this section.

If all the equations for each type of medium are put in matrix form, the resulting equation is $[A]x = b$ where the variables associated with transmitted sound are in the unknown vector x, and the variables associated with incident sound are in the vector b. This allows the matrices for each portion of the panel to be cascaded together in order to get the complete panel matrix. This approach is identical to transmission line theory in electrical power transmission and is also called four-terminal (or four-pole) network theory.

In the case of a single panel with a normally incident plane wave with geometry shown in Figure 1, the pressure and displacement variables can be written as

$$p_i(x,t) = P_i e^{\jmath(\omega t - k_1 x)} \quad (21)$$

$$p_r(x,t) = P_r e^{\jmath(\omega t + k_1 x)} \quad (22)$$

$$p_t(x,t) = P_t e^{\jmath(\omega t - k_2 x)} \quad (23)$$

$$\xi(x,t) = \Xi e^{\jmath\omega t} \quad (24)$$

where the p's are pressures, ξ is displacement, $k_1 = \frac{\omega}{c_1}$, $k_2 = \frac{\omega}{c_2}$, ω is the frequency in radians per second and the c's are the speeds of sound in the media on both sides of the panel. The subscripts i, r and t denote incident, reflected and transmitted waves, respectively. The capital letters P and Ξ are the pressure and displacement magnitudes of the acoustic wave at frequency ω and wave number k, respectively. The total pressure in medium 1 is the sum of the incident and reflected waves or

$$p_1 = p_i + p_r \quad (25)$$

and the total pressure in medium 2 is the pressure from the transmitted wave. At the interface between the air and the panel, there is continuity of displacement. The displacement continuity coupled with the linearized Euler's equation

$$-\nabla p = \rho_o \frac{\partial u}{\partial t} \quad (26)$$

(where ρ_o is the ambient air density and u is the displacement of the acoustic medium) can be used to get the relationship between pressure and panel displacement for a periodic excitation,

$$\nabla p = \rho_o \omega^2 \xi. \quad (27)$$

Combining this relationship and equations (24) and (25) gives

$$P_i - P_r = j\omega\rho_1 c_1 \Xi \tag{28}$$

and

$$P_t = j\omega\rho_2 c_2 \Xi. \tag{29}$$

The equation of motion of the panel is

$$m\ddot{\xi} + \eta\dot{\xi} + \kappa\xi = p_1(0,t) - p_2(0,t) \tag{30}$$

where m is the mass per unit area of the panel, η is the damping co-efficient of the panel and κ is the stiffness of the panel. Combining equations (24), (25), (28), (29), and (30) produces

$$j\omega\Xi(j\omega m + \eta + \frac{\kappa}{j\omega} + \rho_1 c_1 + \rho_2 c_2) = (z_p + z_{f_1} + z_{f_2})j\omega\Xi = 2P_i \tag{31}$$

where the panel impedance is $z_p = j\omega m + \eta + \frac{\kappa}{j\omega}$ and the impedance due to fluid loading on side i is $z_{f_i} = \rho_i c_i$.

For plane waves, the transmission co-efficient is defined as

$$\tau = \frac{\frac{|P_t|^2}{2\rho_2 c_2}}{\frac{|P_i|^2}{2\rho_1 c_1}}, \tag{32}$$

and the reflection co-efficient is

$$r = \frac{|P_r|^2}{|P_i|^2}. \tag{33}$$

From equations (28), (29), (31), (32), and (33) τ can be shown to be

$$\tau = 4\frac{\rho_1 c_1}{\rho_2 c_2}\frac{|z_{f_2}|^2}{|z_{f_1} + z_p + z_{f_2}|^2} \tag{34}$$

and r can be shown to be

$$r = \frac{|-z_{f_1} + z_p + z_{f_2}|^2}{|z_{f_1} + z_p + z_{f_2}|^2}. \tag{35}$$

As a special case consider a massive limp panel with the same air medium on each side or $\rho c = \rho_1 c_1 = \rho_2 c_2 \ll m$, $\kappa = 0$, and $\eta = 0$. In this case the transmission loss is given by

$$\tau = \left(\frac{2\rho c}{\omega m}\right)^2 \tag{36}$$

which is the classical mass law formula for plane waves at normal incidence.

3.2.3 Matrix Formulation

Consider the same panel again. At the interfaces between the panel and the acoustic medium, the variables of interest are the net pressure and the velocity or displacement. The velocities u on each side of the panel are the same or

$$u_1 = u_2 \quad (\xi_1 = \xi_2). \tag{37}$$

The equation of motion of the plate relates the pressures on either side of the panel and can be written as

$$z_p u_{2(or1)} = p_1 - p_2. \tag{38}$$

Equations (37) and (38) can be written in matrix form as

$$\begin{Bmatrix} p_1 \\ u_1 \end{Bmatrix} = \begin{bmatrix} 1 & z_p \\ 0 & 1 \end{bmatrix} \begin{Bmatrix} p_2 \\ u_2 \end{Bmatrix}. \tag{39}$$

At this point equations (28), (29), and (39) can be used to derive τ and r with the same results as before. If the panel design is modified by addition of another layer of different material for example, another equation could be written

$$\begin{Bmatrix} p_2 \\ u_2 \end{Bmatrix} = \begin{bmatrix} 1 & z_{p_2} \\ 0 & 1 \end{bmatrix} \begin{Bmatrix} p_3 \\ u_3 \end{Bmatrix} \tag{40}$$

and by substituting equation (40) into (39)

$$\begin{Bmatrix} p_1 \\ u_1 \end{Bmatrix} = \begin{bmatrix} 1 & z_p \\ 0 & 1 \end{bmatrix} \begin{bmatrix} 1 & z_{p_2} \\ 0 & 1 \end{bmatrix} \begin{Bmatrix} p_3 \\ u_3 \end{Bmatrix} \tag{41}$$

$$= \begin{bmatrix} 1 & z_p + z_{p_2} \\ 0 & 1 \end{bmatrix} \begin{Bmatrix} p_3 \\ u_3 \end{Bmatrix}. \tag{42}$$

In general the total panel matrix can be built up of several two-by-two matrices, one for each separate medium used to make the panel. These matrices are all multiplied together in the order of appearance in the panel. For example, a double wall panel with an air gap (Figure 2) would have an equation with three two by two matrices multiplied together such as

$$[TotalPanelMatrix]^{(2\times2)} = [FirstPanel]^{(2\times2)}[Air]^{(2\times2)}[SecondPanel]^{(2\times2)} \tag{43}$$

Once multiplied together the total panel matrix will be a non-symmetric complex two-by-two matrix and the algorithm for getting τ and r will be identical for any panel design. This method of organizing the equations simplifies coding the equations for maximum flexibility in panel design. Also it is easy to include new types of materials

in the analysis because the only new equation that needs to be derived is the matrix equation which describes the behavior in the new medium.

The transmission and reflection co-efficients can be calculated from their definitions (equations (32) and (33)), the total panel matrix and from Euler's equation (26). The panel matrix equation may be written as follows:

$$\begin{Bmatrix} p_1 \\ u_1 \end{Bmatrix} = \begin{bmatrix} P_{11} & P_{12} \\ P_{21} & P_{22} \end{bmatrix} \begin{bmatrix} A_{11} & A_{12} \\ A_{21} & A_{22} \end{bmatrix} \begin{bmatrix} P'_{11} & P'_{12} \\ P'_{21} & P'_{22} \end{bmatrix} \begin{Bmatrix} p_4 \\ u_4 \end{Bmatrix} \tag{44}$$

where the matrices $[P_{ii}]$ and $[P'_{ii}]$ are four-pole representation of panels 1 and 2 respectively, and the matrix $[A_{ii}]$ defines the air gap between the two panels.

The total panel equation can be rewritten in the following form:

$$\begin{Bmatrix} p_1 \\ u_1 \end{Bmatrix} = \begin{bmatrix} T_{11} & T_{12} \\ T_{21} & T_{22} \end{bmatrix} \begin{Bmatrix} p_n \\ u_n \end{Bmatrix} \tag{45}$$

where p_n and u_n are the pressure and velocity at the panel surface in the last (nth) medium, respectively. The other equations lead to

$$p_1 = p_i + p_r \tag{46}$$

$$p_i|_{x=0} - p_r|_{x=0} = z_{f_1} u_1 \tag{47}$$

$$p_n = p_t \tag{48}$$

$$p_t = z_{f_n} u_n. \tag{49}$$

After solving for the relationship between p_t and p_i and for the relationship between p_r and p_i, it is easy to get transmission and reflection co-efficients by substituting into their definitions,

$$\tau = \frac{z_{f_1}}{z_{f_n}} \left(\frac{4}{\left| T_{11} + \frac{T_{12}}{z_{f_n}} + z_{f_1} T_{21} + \frac{z_{f_1}}{z_{f_n}} T_{22} \right|^2} \right) \tag{50}$$

and

$$\tau = \left(\frac{\left| T_{11} + \frac{T_{12}}{z_{f_n}} - z_{f_1} T_{21} - \frac{z_{f_1}}{z_{f_n}} T_{22} \right|^2}{\left| T_{11} + \frac{T_{12}}{z_{f_n}} + z_{f_1} T_{21} + \frac{z_{f_1}}{z_{f_n}} T_{22} \right|^2} \right) \tag{51}$$

where z_{f_1} is the acoustic impedance of the air at the surface of the panel on side 1, z_{f_n} is the acoustic impedance of the air at the surface of the panel on the transmitting side of the panel (transmits into the nth medium) and T_{ij} is an element of total panel matrix.

The air impedances are ρc for normal incidence, but for oblique incidence and other complicating factors such as air flow the impedance changes. The impedance of plane waves in air with flow at oblique incidence is [9]

$$z_{f_i} = \frac{\rho_i c_i}{\sin\phi_i(1 + M\cos\beta\cos\phi_i)} \tag{52}$$

where M is the Mach number of the flow, ϕ is the angle of incidence with respect to a vector normal to the panel surface and β is the angle between the flow direction and the projection of the wave propagation on the panel surface.

The matrix for an air gap between two panels is [5]

$$\begin{bmatrix} \cos(k_i d_i \cos(\phi_i)) & \jmath z_{f_i} \sin(k_i d_i \cos(\phi_i)) \\ \jmath \sin(k_i d_i \cos(\phi_i))/z_{f_i} & \cos(k_i d_i \cos(\phi_i)) \end{bmatrix} \tag{53}$$

where d_i is the depth of the air gap, z_{f_i} is the acoustic impedance in the air gap, ϕ_i is the angle of sound propagation with respect to a vector normal to the panel and k_i is the wave number of sound in the air gap.

The matrix for a fiberglass layer is given by [5]:

$$\begin{bmatrix} \cosh(qd_m) & \jmath Z_{m_x} \sinh(qd_m) \\ \jmath \sinh(qd_m)/Z_{m_x} & \cosh(qd_m) \end{bmatrix} \tag{54}$$

where d_m is thickness of the fiberglass blanket. The propagation constant q and the characteristic acoustic impedance Z_{m_x} of the fiberglass material in the x-direction are given by [6]:

$$q = \gamma_m \sqrt{1 - \frac{\jmath k sin\phi_i}{\gamma_m}} \tag{55}$$

$$Z_{m_x} = \frac{\gamma_m Z_m}{q} \tag{56}$$

The propagation constant γ_m and the characteristic impedance Z_m may be presented as a function of the dimensionless parameter $\frac{\rho f}{R_1}$:

$$\gamma_m = \alpha_m + \jmath\beta_m \tag{57}$$

where

$$Z_m = R_m + \jmath X_m \tag{58}$$

$$\alpha_m = \frac{\omega}{c}[0.189(\frac{\rho f}{R_1})^{-0.595}] \tag{59}$$

$$\beta_m = \frac{\omega}{c}[1 + 0.0978(\frac{\rho f}{R_1})^{-0.700}] \tag{60}$$

$$R_m = \rho c[1 + 0.0571(\frac{\rho f}{R_1})^{-0.754}] \tag{61}$$

$$X_m = -\rho c[0.0870(\frac{\rho f}{R_1})^{-0.732}] \tag{62}$$

where R_1 is the flow resistivity (rayls/m) and ρ is the gas density in the ambient medium.

Comparison with experimental data has shown that as a conservative approach, the range over which the above empirical equations for the semirigid materials are valid is [6,7]: $0.01 \leq \frac{\rho f}{R_1} \leq 0.1$. In addition, the lower limiting frequency is determined by $d_m \leq \lambda_m$, where λ_m is the wavelength of sound within the fiberglass blanket ($\lambda_m = \frac{2\pi}{\beta_m}$).

This method of setting up the transmission equations is very attractive due to the flexibility available in panel design and also to the ease of integrating new materials or more detailed analysis of old materials into the transmission loss prediction program.

3.2.4 Mechanical Bridging Effects

When a panel is made up of multiple layers and air gaps, there are usually frames holding the panels in place. This mechanical connection between the panels provides a flanking path for the energy to travel. Thus far only the airborne portion of the path has been considered. In this section a lumped parameter model of the structural path through the frames is developed. The frames are assumed to have periodic, parallel line connections on the panels. This type of connection is like the frames in a standard aircraft sidewall or like the studs in a wall in standard residential housing construction. This development is based on the four-pole (or four terminal) network theory [8]. The four-pole modelling approach permits a complete matrix formulation of a typical aircraft sidewall panel. The effects of fiberglass insulation can also be incorporated.

For simplicity, a connected panel-airgap-panel system, as shown in Figure 3, is considered here. A structural path between the panels is provided by the frames. Two assumptions about the frames are:

- the dynamic behavior of each frame is independent of any other frame
- the frames translate as rigid bodies in their own planes.

The first panel is excited by the acoustic wave driving a bending wave along the panel. When the wave hits a frame, the frame scatters the wave. Also the frame is

driven by the deflection of the first panel. The frame excites the second panel which radiates the sound. The structural sound path is assumed to be independent of the acoustic path.

Neglecting the fluid loading effects, the bending wave velocity of the first panel is

$$\jmath\omega\xi_1 \approx \frac{2p_i}{\jmath\omega m_1}, \tag{63}$$

where ξ_1 is the displacement of the first panel, p_i is the pressure incident on the panel, m_1 is the mass per unit area of the first panel and ω is the frequency in radians per second. The velocity of a frame (line mass) when driven by a bending wave in a panel is

$$\jmath\omega\xi_f = \frac{\jmath\omega\xi Z_{F_1}}{(Z_{F_1} + \jmath\omega m_f + Z_{F_2})}, \tag{64}$$

where ξ_f is the displacement of the frame, m_f is the mass per unit length of the frame, $Z_{F_i} = 2D_i^{1/4}\omega^{1/2}m_i^{3/4}(1+\jmath)$ is the line force impedance of panel i and D is the bending stiffness of panel i.

The bridging impedance due to the mass of the frame and the line force impedances of the panels is therefore:

$$Z_b = Z_{F_1} + \jmath\omega m_f + Z_{F_2} \tag{65}$$

In the four-pole representation of the connected panel system the bridging path (through the frame) can be considered as a shunt element, Z_b, parallel to the airgap impedance, Z_a. The force at the input point of the parallel connection is same as that at its output terminal. The total panel matrix for calculating transmission loss of such a panel configuration may now be written as follows:

$$\begin{Bmatrix} p_1 \\ u_1 \end{Bmatrix} = \begin{bmatrix} P_{11} & P_{12} \\ P_{21} & P_{22} \end{bmatrix} \begin{bmatrix} \beta_{11} & \beta_{12} \\ \beta_{21} & \beta_{22} \end{bmatrix} \begin{bmatrix} P'_{11} & P'_{12} \\ P'_{21} & P'_{22} \end{bmatrix} \begin{Bmatrix} p_4 \\ u_4 \end{Bmatrix} \tag{66}$$

where the $[\beta]$ matrix describes the four-pole parameters of the parallel connection. These parameters can be determined using matrix techniques [8].

The matrix equation for a general case of n impedances connected in parallel may be written as follows:

$$\begin{Bmatrix} p_2 \\ u_2 \end{Bmatrix} = \begin{bmatrix} \beta_{11} & \beta_{12} \\ \beta_{21} & \beta_{22} \end{bmatrix} \begin{Bmatrix} p_3 \\ u_3 \end{Bmatrix} \tag{67}$$

where

$$\beta_{11} = \frac{A}{B} \tag{68}$$

$$\beta_{22} = \frac{C}{B} \tag{69}$$

$$\beta_{12} = \frac{AC}{B} - B \tag{70}$$

$$\beta_{21} = \frac{1}{B} \tag{71}$$

$$A = \sum_{i=1}^{n} \left(\frac{\alpha_{11}^i}{\alpha_{21}^i} \right) \tag{72}$$

$$B = \sum_{i=1}^{n} \left(\frac{1}{\alpha_{21}^i} \right) \tag{73}$$

$$C = \sum_{i=1}^{n} \left(\frac{\alpha_{22}^i}{\alpha_{21}^i} \right) \tag{74}$$

3.3 Validation

The transmission loss prediction method presented in Section 3.2 was validated using laboratory data on test panels. The measured TL data for bare and treated stiffened flat test panels (dimensions: $1.46m \times 2.3m \times 12mm$), which are representative of an aircraft fuselage sidewall, were used for the validation.

The predicted transmission loss of the bare test panel is compared with the laboratory test data in Figure 4. The TL of the test panel is underpredicted at low and mid-frequencies. Since the prediction model is based on the infinite panel theory, it does not account for the (two-dimensional) stiffening effect of frames and longerons on the test panel.

The measured TL of the same test panel with fiberglass insulation (blanket thickness: 76.2mm) and a 1mm thick trim panel is compared with the predicted TL in Figure 5. The acoustic absorption effects due to fiberglass insulation were included in the predictions. The predicted TL is seen to be in good agreement with the test data.

The comparisons of the predicted TL of a typical aircraft sidewall panel with laboratory data therefore validates the TL prediction module.

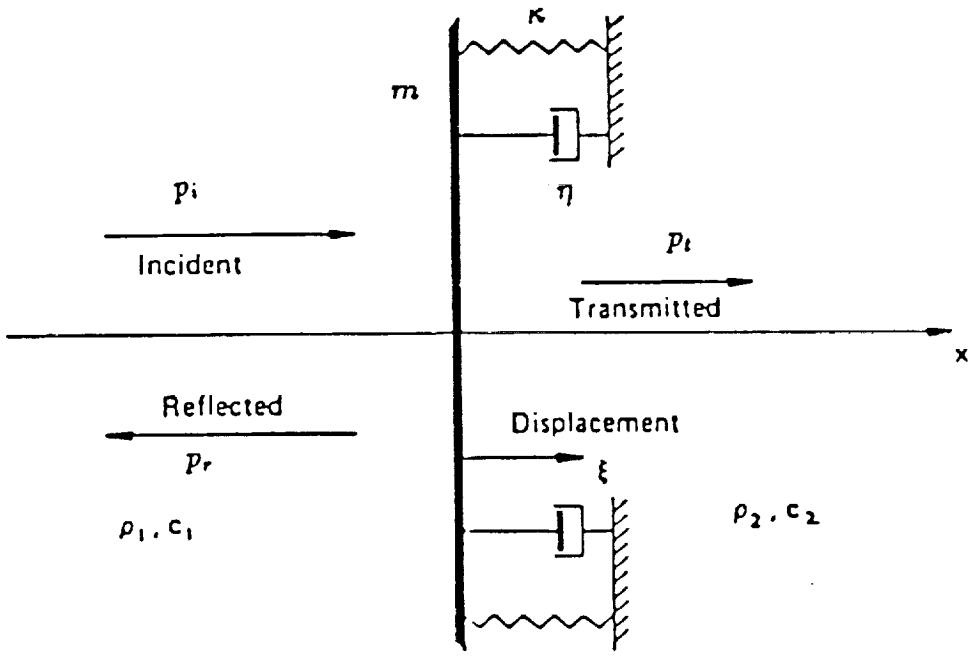

Figure 1: Geometry of normally incident plane wave on a single panel

$$\begin{Bmatrix} p_1 \\ u_1 \end{Bmatrix} = \begin{bmatrix} P_{11} & P_{12} \\ P_{21} & P_{22} \end{bmatrix} \begin{bmatrix} A_{11} & A_{12} \\ A_{21} & A_{22} \end{bmatrix} \begin{bmatrix} P'_{11} & P'_{12} \\ P'_{21} & P'_{22} \end{bmatrix} \begin{Bmatrix} p_2 \\ u_2 \end{Bmatrix}$$

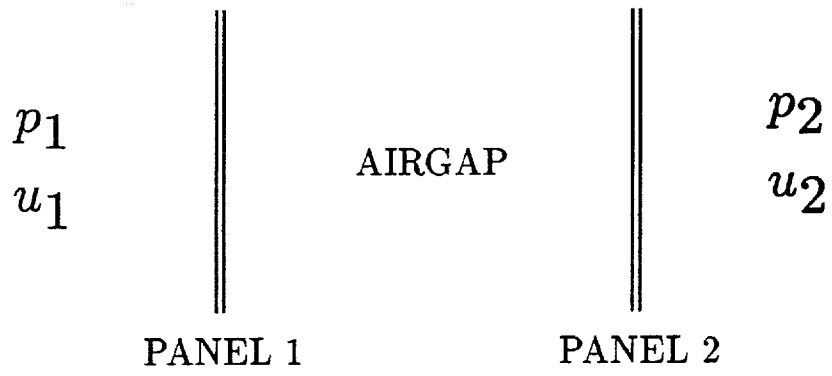

Figure 2: Equivalent Transmission Loss Matrix Representation of Panel-Airgap-Panel System

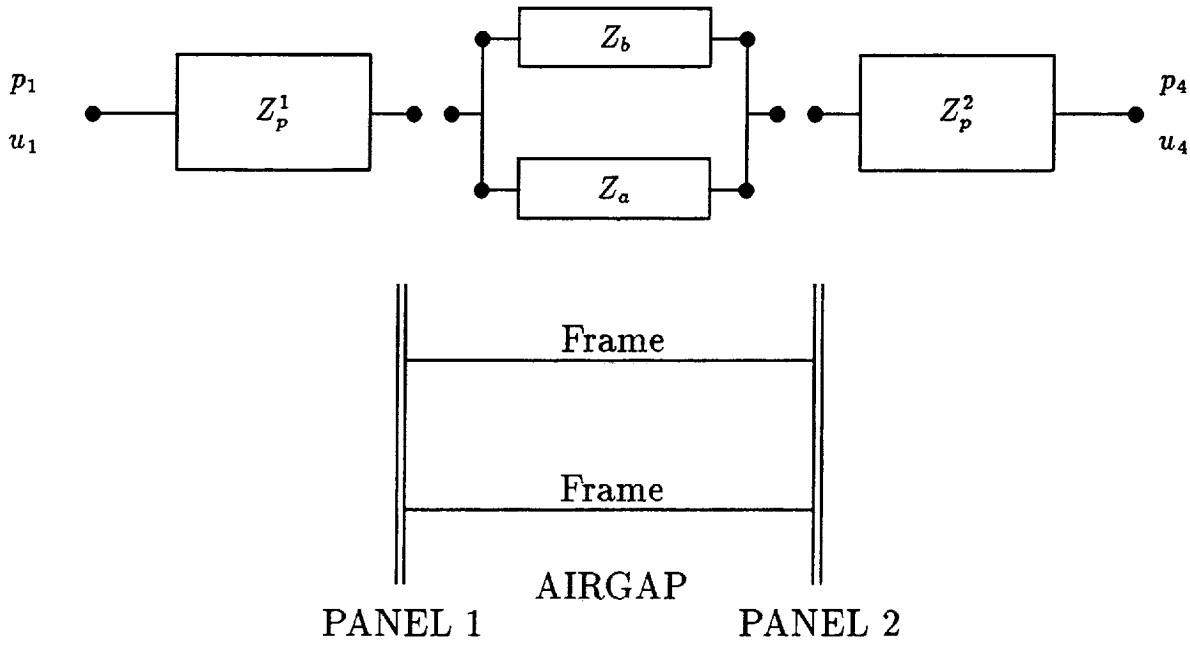

Figure 3: Equivalent Impedance Representation of Panel-Airgap-Panel System with Structural Bridging

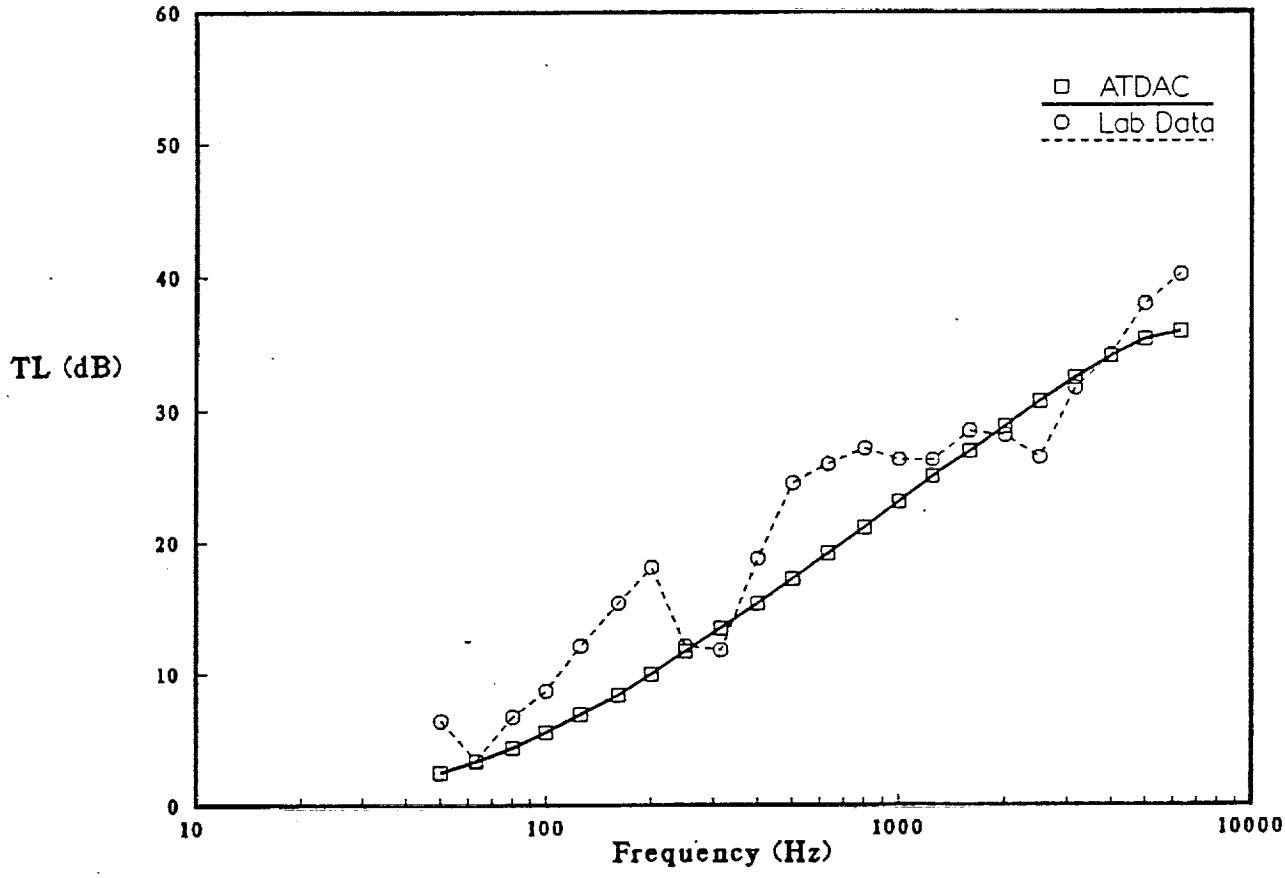

Figure 4: Comparison of Predicted Transmission Loss of a Flat Sidewall Panel with Laboratory Data - Panel Thickness: 0.00127 m

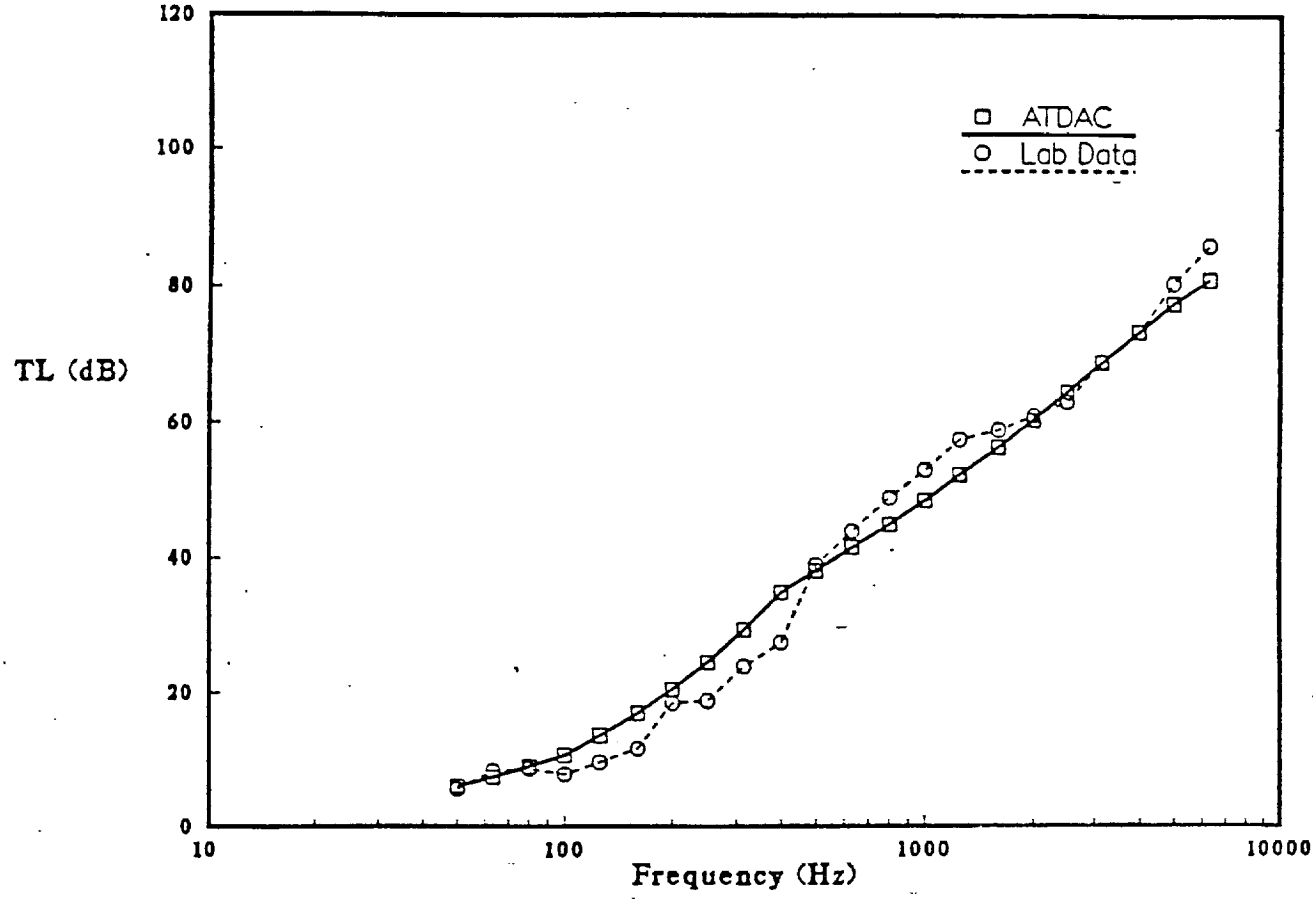

Figure 5: Predicted vs. Measured Transmission Loss Data of a Flat Sidewall Panel (.00127 m) with Fiberglass Insulation (0.0762 m) and Trim Panel (0.00076 m)

4 Structure-Borne Noise Models

4.1 Structure-Borne Noise Overview

The structure-borne noise models were developed to predict the engine noise that is transmitted from the engine to the fuselage through a structural path (as opposed to an airborne path which impinges on the structure). The vibration of the engine is transmitted through the pylon (or wing) to the fuselage which radiates sound into the cabin. The inputs necessary to make this prediction are the forces of the engine acting at the engine mounts and the physical or statistical parameters which describe the pylon/fuselage region.

The structure-borne path was separated into two regions. The first region (Region I) covers the path of the vibrational energy from the engine to the vibrational energy in the fuselage. The second region (Region II) covers the radiation of the fuselage vibrational energy into acoustical energy in the cabin. The energy radiated into the cabin is input into the energy balance equation as an additional energy source.

For both regions, there are two alternative analysis procedures which may be used. In the first region the vibrational energy of the fuselage may be determined with either a simple SEA model of the pylon(or wing)/fuselage connection or a user defined transfer function. In the second region, the acoustical radiation from the fuselage may be predicted with either the radiation efficiency formula for flat plates or a user defined transfer function.

4.2 SEA Model

Since the Statistical Energy Analysis (SEA) approach is based on the overall statistical properties of energy flow, complex structures may be modelled by simple idealized structural elements with equivalent statistical properties. When using the SEA technique, the dynamic system being studied is divided into a set of connected substructures. SEA substructures are typically simple structural/fluid element representations, such as beams, plates, acoustic spaces etc., for sections of the modelled system. Each substructure is then divided into subsystems which are groups of modes having similar dynamic characteristics. The power balance equations are then set up by balancing the time average net vibratory power input to each subsystem with the time average power dissipated within the subsystem and the power transferred to other subsystem(s). Vibratory energy flow between subsystems is controlled by equations analogous to the equations for steady state heat or fluid flow. Energy flow between subsystems is proportional to the difference in subsystem modal energies. The input excitation for the

SEA model is applied as the power input to the specified subsystem. The power balance equations are then solved for the modal energies within the subsystems. The response variables of interest for the specified subsystem are determined from the modal energies.

In order to keep the prediction scheme simple and general in scope so that it is appropriate for both wing and pylon mounted engines, the pylon/fuselage region is modelled as a two element SEA system. Each element of the SEA system is represented by an equivalent flat plate. An equivalent flat plate is defined as a flat plate with statistical properties (such as modal density) the same as the pylon or fuselage structure. The pylon's equivalent plate is rigidly connected perpendicularly to the fuselage's equivalent plate. Engine vibration data are input to the pylon element and the SEA power flow equations are solved to give the space-averaged velocity in the fuselage which will be the input to the radiation model in Region II.

The equations for power balance in SEA involve certain parameters defining the energy flow between subsystems, called "coupling loss factors". The coupling loss factor is a measure of intermodal forces between the interacting multimodal systems, averaged over frequency and over the modes of the interacting systems. In addition, each SEA subsystem is statistically described by the following parameters: mode count $N(\omega)$, wavenumber $k(\omega)$, and damping loss factor η.

The steady state power balance equations for the case of two coupled subsystems are given by (see Figure 6) [11]

$$\Pi_1^{in} = \Pi_1^{dis} + \Pi_{12} \tag{75}$$

$$\Pi_2^{in} = \Pi_2^{dis} - \Pi_{12}. \tag{76}$$

The power dissipated in each subsystem is given by

$$\Pi_i^{dis} = \omega E_i^m \eta_i, \tag{77}$$

and the net power flow from subsystem 1 to 2 is given by

$$\Pi_{12} = \Pi_{12}{}' - \Pi_{21}{}', \tag{78}$$

where $\Pi_{ij}{}'$ is the power transmitted from subsystem i to subsystem j. Π_1^{in} denotes the input power to subsystem 1 and E^m represents the average subsystem modal energy,

$$E^m = \frac{E}{N(\omega)}, \tag{79}$$

where E is the total energy of the subsystem.

The net power transmitted from subsystem 1 to subsystem 2 is proportional to the difference in subsystem modal energies and may be expressed as

$$\Pi_{12} = \omega\eta_{12}N_1(\omega)[E_1^m - E_2^m], \tag{80}$$

where E_1^m and E_2^m are the average modal energies of subsystems 1 and 2 respectively.

In matrix form, the power balance equations are

$$\omega \begin{bmatrix} (\eta_1 + \eta_{12})N_1(\omega) & -\eta_{21}N_2(\omega) \\ -\eta_{12}N_1(\omega) & (\eta_2 + \eta_{21})N_2(\omega) \end{bmatrix} \begin{Bmatrix} E_1^m \\ E_2^m \end{Bmatrix} = \begin{Bmatrix} \Pi_1^{in} \\ \Pi_2^{in} \end{Bmatrix}. \tag{81}$$

There are essentially four parameters that enter into the SEA prediction scheme: (1) mode count, (2) coupling loss factor, (3) dissipative loss factor, and (4) input power. The mode count, $N(\omega)$, of a subsystem is defined as the number of resonant modes within a given frequency band. The mode count for transverse vibrations of a homogeneous rectangular panel is given by [11]

$$N_i(\omega) = \frac{\omega S_{p_i}}{4\pi\kappa_{p_i}c_{l_i}} \tag{82}$$

where S_{p_i} is the surface area of plate i, $\kappa_{p_i} = \frac{h_i}{\sqrt{12}}$ is radius of gyration, $c_{l_i} = \sqrt{\frac{E_i}{\rho_i(1-\nu_i^2)}}$ is longitudinal wave speed, ν_i is the Poisson's ratio for plate material and ρ_i is the material density (mass per unit volume).

The coupling loss factor describes the power flow from one subsystem to another. In the present case, the coupling is in the form of a mechanical connection between two structural elements. In the case of two plates connected at right angles, the coupling loss factor, η_{12}, is related to the random incidence transmission co-efficient, τ_{ij}^R, by [12]

$$\eta_{ij} = \frac{2L_{ij}}{\pi k_i S_{p_i}}\tau_{ij}^R, \tag{83}$$

where L_{ij} is the length of the coupling line and k_i is the bending wavenumber in plate i.

The random incidence transmission co-efficient, τ_{ij}^R, is [13]

$$\tau_{ij}^R \approx \frac{2}{[X^{5/4} + X^{-5/4}]^2} \cdot \frac{2.754X}{1 + 3.24X} \tag{84}$$

where $X = h_i/h_j$, h_i is the thickness of panel i and h_j is the thickness of panel j.

The predicted modal energy of a subsystem can be transformed into physical parameters, such as spatially averaged vibration velocity, $< v >$ by

$$< |v|^2 > = \frac{E^m N(\omega)}{\rho_s S_p}, \tag{85}$$

where ρ_s is the mass per unit area of the structural element.

The mechanical input power injected into a structure by external sources is one of the parameters that is presumed known in the SEA prediction scheme. The input power at a given frequency or in a band of frequencies may be defined in terms of the input mobility function as follows

$$\Pi_1^{in} = \frac{1}{2}|F|^2 Re\{Y(\omega, x_o)\} = \frac{1}{2}|V|^2 \frac{Re\{Y(\omega, x_o)\}}{|Y(\omega, x_o)|^2}, \tag{86}$$

where $Y(\omega, x_o)$ is the input mobility of the structure at the driving point x_o and may be defined as the complex ratio of the velocity vector $V(\omega, x_o)$ to the force vector $F(\omega, x_o)$

$$Y(\omega, x_o) = \frac{V(\omega, x_o)}{F(\omega, x_o)}, \tag{87}$$

and $Re\{..\}$ indicates the real part of the argument function.

The input mobility and the input force or velocity are used to calculate the input power as in equation (86). The physical parameters of the equivalent plate are used in equations (82)-(84) to calculate the terms in the SEA matrix equation (81). By solving equation (81), the power in the fuselage is found and may be used to calculate the space average velocity by equation (85). The space average velocity is then input to the radiation module (Region II).

4.3 Radiation Efficiency Model

The original work which defined the radiation efficiency of stiffened panels was done by Maidanik [14]. The form used in this analysis was presented by Vér and Holmer [3] . The acoustical power, Π, radiated by a flat plate subjected to a random incident, uniform acoustical loading is given by

$$\Pi(\omega) = \epsilon(\omega)\rho c S < |v(\omega)|^2 > \tag{88}$$

where ϵ is the average radiation co-efficient as a function of frequency, ρ is the density of the medium the panel is radiating into, c is the speed of sound in the same medium, S is the area of the radiating surface, and $< v(\omega) >$ is the space averaged velocity of the plate at frequency ω.

The average radiation co-efficient, ϵ, is defined differently in four separate frequency regions. These regions are: well below coincidence, below coincidence, at coincidence

and above coincidence. The coincidence frequency is:

$$\omega_c = c^2\sqrt{\frac{\rho_s}{D}} \tag{89}$$

where $D = \frac{Eh^3}{12(1-\nu^2)}$ is the bending stiffness, c is the speed of sound in the radiating medium, $\rho_s = \rho h$ is the mass per unit area of the panel, ρ is the density of the panel, h is the thickness of the panel, E is Young's modulus of the panel and ν is Poisson's ratio of the panel.

In the four frequency regions, the average radiation co-efficient ϵ is defined as follows:

$$\epsilon(\omega) = \frac{S}{\pi^2 c^2}\omega^2 \quad when \quad \omega < \omega_c \; and \; \omega < \frac{2\sqrt{12D}}{h\sqrt{\rho_s}(MAX(l_x, l_y))} \tag{90}$$

and

$$\epsilon(\omega) = \frac{\lambda_c^2}{S}g_1(\sigma) + \frac{P\lambda_c}{S}g_2(\sigma) \quad when \quad \omega_c > \omega > \frac{2\sqrt{12D}}{h\sqrt{\rho_s}(MAX(l_x, l_y))}; \tag{91}$$

$$\epsilon(\omega) \approx \left(\frac{l_x}{\lambda_c}\right)^{1/2}\left(\frac{l_y}{\lambda_c}\right)^{1/2} \quad when \quad \omega = \omega_c; \tag{92}$$

$$\epsilon(\omega) \approx \left(1 - \frac{\omega_c}{\omega}\right)^{-1/2} \quad when \quad \omega > \omega_c; \tag{93}$$

where

$$\sigma = \left(\frac{\omega}{\omega_c}\right)^{1/2}, \tag{94}$$

$$g_1(\sigma) \;=\; \begin{cases} \frac{8}{\pi^4}\frac{(1-2\sigma^2)}{\sigma(1-\sigma^2)^{1/2}} & if \; \omega < \omega_c/2 \\ 0 & if \; \omega > \omega_c/2 \end{cases}, \tag{95}$$

$$g_2(\sigma) = \frac{1}{4\pi^2}\left[\frac{(1-\sigma^2)\ln(\frac{1+\sigma}{1-\sigma}) + 2\sigma}{(1-\sigma^2)^{3/2}}\right], \tag{96}$$

$$P = 2[l_x(1 + N_{sx}) + l_y(1 + N_{sy})], \tag{97}$$

$\lambda_c = \frac{2\pi}{c}\sqrt{\frac{D}{\rho_s}}$ is the bending wavelength, N_{sx} is the number of lengthwise stiffeners, N_{sy} is the number of widthwise stiffeners, l_x is the length of the panel and l_y is the width of the panel.

The radiation co-efficient ϵ is calculated from the physical plate parameters of the radiating surface using equations (90) to (97). The radiation co-efficient together with the space-averaged velocity, equation (85) from Region I is used in equation (88) to calculate the power radiated from the plate. The radiated power is then input into the room equation as an interior power source.

4.4 Transfer Function Models

The transfer function approach brings flexibility to the analysis of the structure-borne path. Experimental data or theoretical data from an alternative analysis may be included by the use of transfer functions. The transfer function equation for the first path (Region I) which is from the engine force to the fuselage vibration is

$$F(\omega) \times H_I(\omega) = v(\omega), \tag{98}$$

where F is the engine force on the pylon, ω is the frequency in radians per second, H_I is the transfer function for Region I and v is the velocity of the fuselage. Both the engine force F and the transfer function H_I are input by the user and the fuselage velocity v is the output to be used in Region II.

The transfer function equation for the second path (Region II) which is from the the fuselage vibrational velocity to the radiated acoustical power is

$$v(\omega) \times H_{II}(\omega) = \Pi(\omega), \tag{99}$$

where v is the velocity of the fuselage, ω is the frequency in radians per second, H_{II} is the transfer function for Region II and $\Pi(\omega)$ is the acoustical power radiated into the cabin. In this region, the fuselage velocity v is the result from Region I, or from SEA model, equation (85) the transfer function H_{II} is input by the user, and the acoustical power $\Pi(\omega)$ computed by equation (99) is input into the room equation as an alternate source of energy.

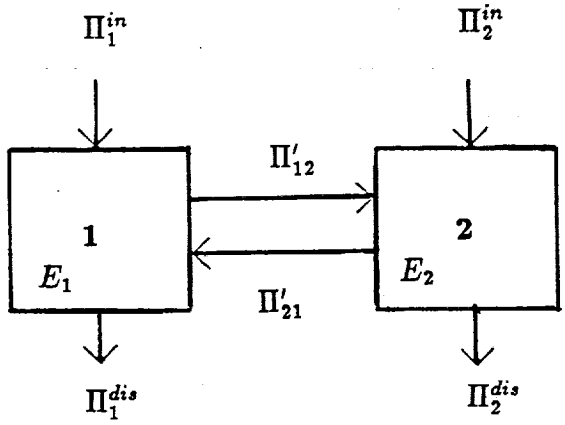

Figure 6: Power Flow Between Two Sets of Linearly Coupled Subsystems

5 Boundary Layer Noise Model and Validation

5.1 Prediction Model

The pressure fluctuations in the turbulent boundary layer caused by the airflow past the aircraft are one of the main sources of cabin noise. The turbulent boundary layer prediction scheme used in ATDAC is based on empirical formulae derived by Lowson [15].

The overall root mean square pressure fluctuation of the spectrum, p_{rms}, is given by the empirical equation

$$\frac{p_{rms}}{q} = \frac{0.006}{1 + 0.14M^2,} \tag{100}$$

where $q = \frac{1}{2}\rho_o U^2$ is the dynamic pressure head, ρ_o is the air density, $U = cM$ is the aircraft velocity, c is the speed of sound and M is aircraft Mach number. The power spectral density is defined by another empirical equation

$$p(\omega)^2 = \frac{p_{rms}^2}{\omega_o[1 + (\omega/\omega_o)^2]^{3/2}} \tag{101}$$

where ω is the frequency (rad/sec) and $\omega_o = 8U/\delta$ is a characteristic frequency for normalization purposes. The boundary layer thickness δ is given by an empirical formula suggested by Bies [16]

$$\frac{\delta}{x} = 0.37 Re_x^{-0.2} \left\{1 + (\frac{Re_x}{6.9 \times 10^7})^2\right\}^{0.1} \tag{102}$$

where x is the distance from the nose of the aircraft, $Re_x = Ux/\nu$ is the Reynolds number and ν is the kinematic viscosity. The one-third octave pressure spectrum is calculated from the power spectral density by integrating over each one-third octave band. The power spectral density is assumed to be smooth and fairly slowly varying for integration over each one-third octave band.

5.2 Validation

This empirical model was compared with two sets of experimental data. All the data were non-dimensionalized to simplify the comparison. The magnitude of the measured boundary layer pressure was non-dimensionalized by dividing by $q\sqrt{\frac{\delta}{cM}\frac{1}{(1+0.14M^2)}}$ and the frequency was non-dimensionalized by multiplying by $\frac{\delta}{cM}$. The empirical prediction curve collapses to a single curve when non-dimensionalized in this way. The non-dimensionalized data in Figure 7 for the MD-UHB Demonstrator (which was limited

to frequencies below 2000 Hz before normalization) display a lot of scatter. The data in Figure 8 for the Boeing 737 [17] aircraft show similar results but extend to higher frequencies. In the mid to low frequency region the empirical model seems to provide an upper bound to the range of measurements, but in the higher frequency region the empirical model drops off faster than the measured data. The empirical model is conservative in the mid to low frequency regions and for many noise problems these are the important frequencies.

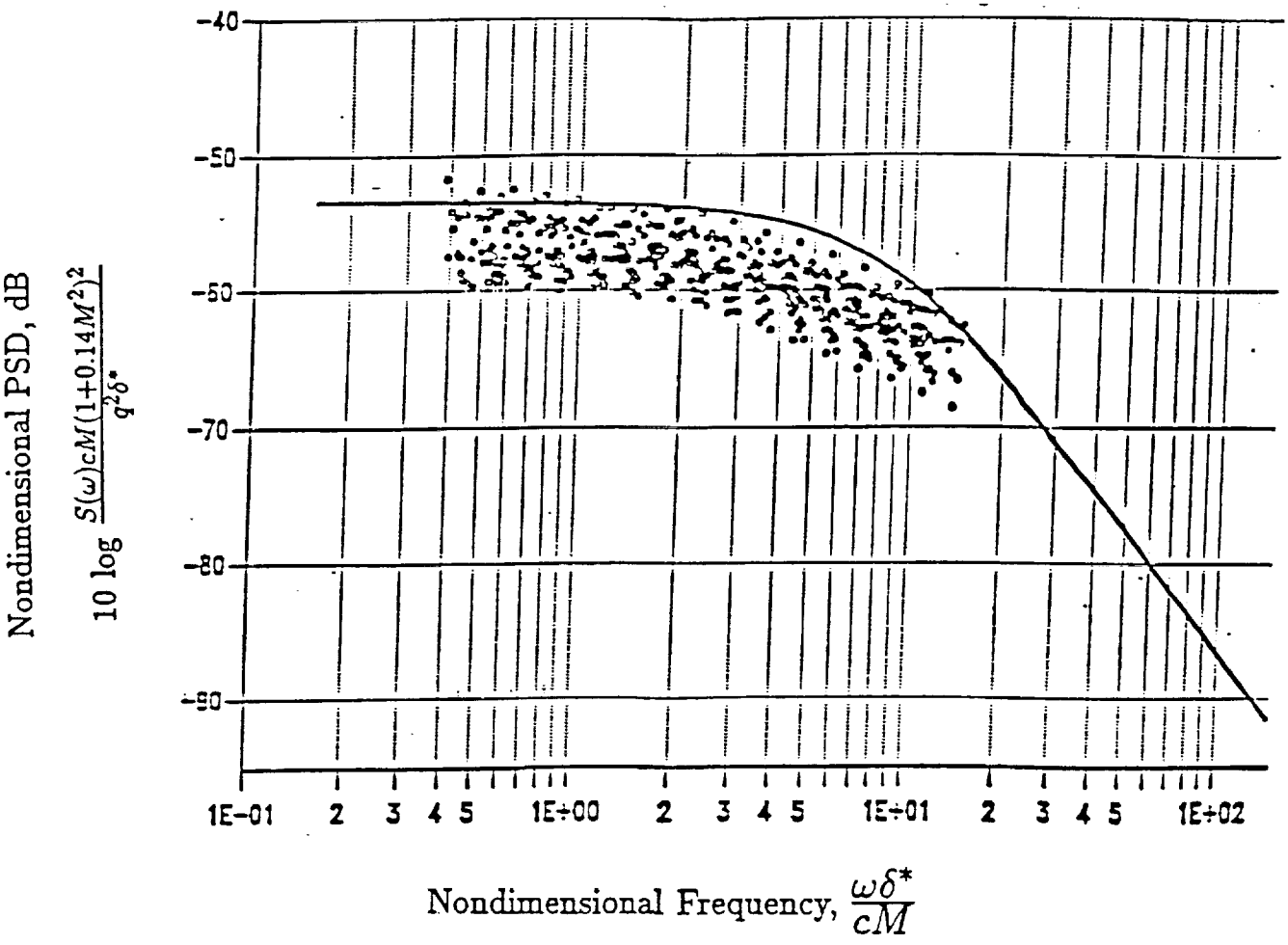

Figure 7: Comparison of Predicted (–) and Measured (○, •) Turbulent Boundary Layer Noise. Measured Data from MD-UHB Demonstrator Aircraft.

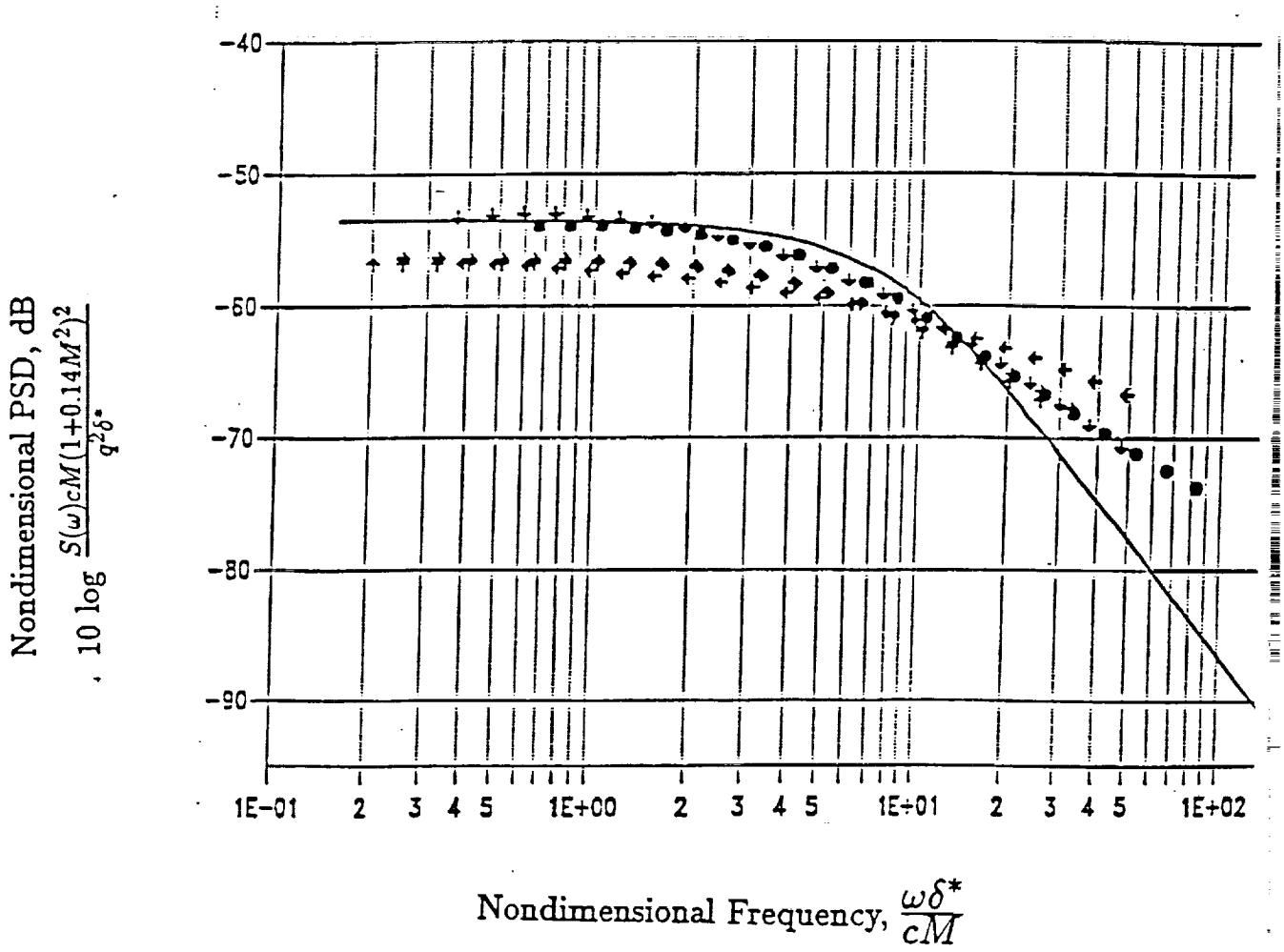

Figure 8: Comparison of Predicted (–) and Measured (←, ↑, ↓, •) Turbulent Boundary Layer Noise. Measured Data from a Boeing 737 Aircraft.

6 Cabin Noise Prediction Validation

The validation of ATDAC involved comparison of predicted transmission loss, boundary layer noise and cabin noise levels with measured data. The transmission loss and boundary layer noise prediction modules were validated with experimental data in Sections 3.3 and 5.2 respectively. In this section, the overall ATDAC interior noise predictions are validated using flight test data for the MD-UHB Demonstrator aircraft. The Demonstrator aircraft is a modified MD-80 series aircraft. The MD-80 aircraft, with an overall length of 147.8 ft and a wing span of 107.8 ft, is designed to carry 155 passengers. The MD-80 aircraft is normally powered by two Pratt & Whitney JT8D-209 engines. The aircraft (ship 909) was modified by replacing the left engine with a General Electric proof-of-concept Unducted fan (UDF) engine.

The validation of ATDAC as an aircraft cabin noise prediction method required complete modelling of the MD-UHB Demonstrator aircraft. The details of aircraft cabin, noise sources and material modelling are given in the User's manual [1]. The aircraft cabin was divided into 47 volumes and 111 exterior surfaces. There were 74 interior partitions, such as the floor and pressure bulkhead, which separated different volumes. In the case of two adjoining volumes with no material surface joining them, an air partition was used. The geometrical details, such as surface areas, global location of each volume and partitions joining different volumes, were generated using the geometry module and stored in a geometry file. The transmission loss and reflection co-efficients of the fuselage surfaces and interior partitions were estimated using the transmission loss module and were stored in a panel database file. The acoustic absorption characteristics of the interior cabin surfaces were contained in absorption files. A material file assigned the acoustical characteristics of the surfaces and partitions according to the geometrical description of the aircraft cabin.

The source file module prepared an output source file which contained information about all the noise sources including exterior boundary layer noise, airborne noise due to the propfan and structure-borne engine noise. The UHB engine used for these flight tests was a General Electric UDF engine with two rows of highly swept, counter rotating propeller blades. The flight test data from an 8×8 engine configuration (consisting of eight blades on both the forward and aft rotors) was used for the ATDAC validation in this report. Interior noise spectra (see Figure 9) in the aft cabin, measured in flight, were found to contain several tones, superimposed on broadband noise. These tones correspond to the blade passage frequencies of the propeller and other engine sources. Tones at the blade passage frequency (BPF) and harmonics are generated by each propeller. These propeller harmonics are labelled as 2BPF, 3BPF etc. An additional tone labeled UN1 is associated with the rotational speed of the low pressure stage of the General Electric UDF engine. The broadband noise is mainly due to exterior boundary

layer noise.

A knowledge of the main noise transmission paths into the aircraft cabin is very useful in modelling various noise sources. Extensive laboratory and flight test investigations conducted on the MD-UHB Demonstrator aircraft provided measured data for ATDAC prediction model and information for modelling noise transmission paths. The following noise transmission paths were modelled:

- an airborne noise path through the cabin sidewall for propeller tones and broadband boundary layer noise component
- a structure-borne transmission path through the engine pylon and the aft fuselage for propeller and engine tones
- a combined airborne/structure-borne path for propeller tones: the tail section is set into vibrations due to acoustic energy from the propeller blades; the aft pressure bulkhead, in turn, is excited by the tail surface and radiates energy into the cabin.

Measured flight test data for the MD-UHB Demonstrator aircraft provided input levels for airborne and structure-borne noise sources [18]. The main structure-borne noise source for cabin noise prediction was simulated using the measured vibration levels at the left aft mount of the UHB engine. Figure 10 shows measured acceleration levels at aft engine mount location for BPF and UN1 tones.

The structure-borne sound transmission from the engine pylon was modelled using the SEA approach described in Section 4. The input power due to structure-borne noise sources was estimated using the drive-point input mobility formulation. In addition to boundary layer noise, propeller tones at blade passage frequencies were simulated as exterior airborne noise sources for the aft fuselage. Figure 11 shows exterior noise spectra on the aft fuselage due to the 8×8 propfan engine. A combined airborne/structure-borne path through the aft fuselage (tail surface) and aft pressure bulkhead was simulated using the transfer function approach. Figure 12 shows BPF vibration and noise levels as a function of rotor speed for a fuselage accelerometer in the forward prop plane and an interior microphone in the unpressurized section aft of the bulkhead.

The cabin noise levels due to exterior airborne noise source, i.e. propeller tones 1BPF and 2BPF, and structure-borne noise sources, i.e., engine tone UN1 and propeller tone 1BPF, were predicted separately. The effect of airborne noise source due to exterior boundary layer noise was not included. The predicted airborne and structure-borne cabin noise components are compared with measured flight test cabin noise levels

in Figure 13. The predicted cabin noise levels (spatially-averaged levels in Row 6 seats) shown in Figure 13 compare well with the measured data. It was found that the combined airborne/structure-borne path, e.g., via aft fuselage (tail section) and pressure bulkhead for 1BPF propeller tone (at 168 Hz) was more dominant than the airborne path.

A comparison of ATDAC predicted cabin noise levels with flight test data for aft cabin locations (Row 6 seats) on the Demonstrator aircraft is shown in Figure 14. The predicted interior noise levels are in good agreement with those measured during flight. The cabin noise levels above 200 Hz 1/3-octave band are mainly controlled by the turbulent boundary layer noise. The structure-borne cabin noise component due to UN1 engine tone in the 200 Hz 1/3-octave band was overshadowed by the airborne contribution from exterior turbulent boundary layer noise. The airborne contribution from 2BPF propeller tone in the 315 Hz 1/3-octave band was similarly masked by the boundary layer noise component. The overestimation of cabin noise levels in the frequency range of 200 and 800 Hz may be attributed to the following: (1) higher exterior boundary layer noise spectrum levels and, (2) lower transmission loss of the fuselage. The predicted cabin noise levels are in very good agreement with the measured data at both low and high frequencies.

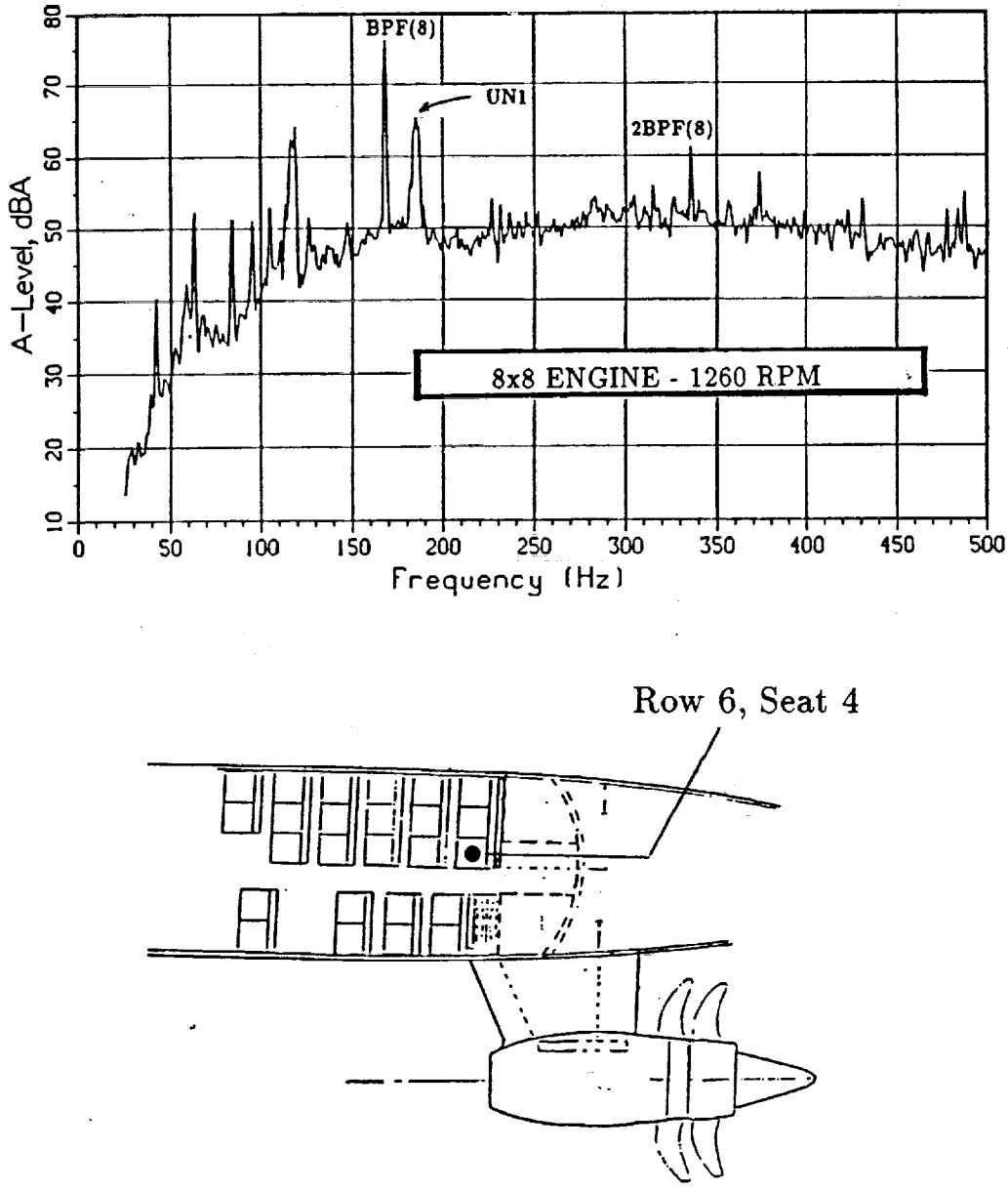

Figure 9: A Typical Interior Cabin Noise Spectrum measured at Row 6, Seat 4 (•)

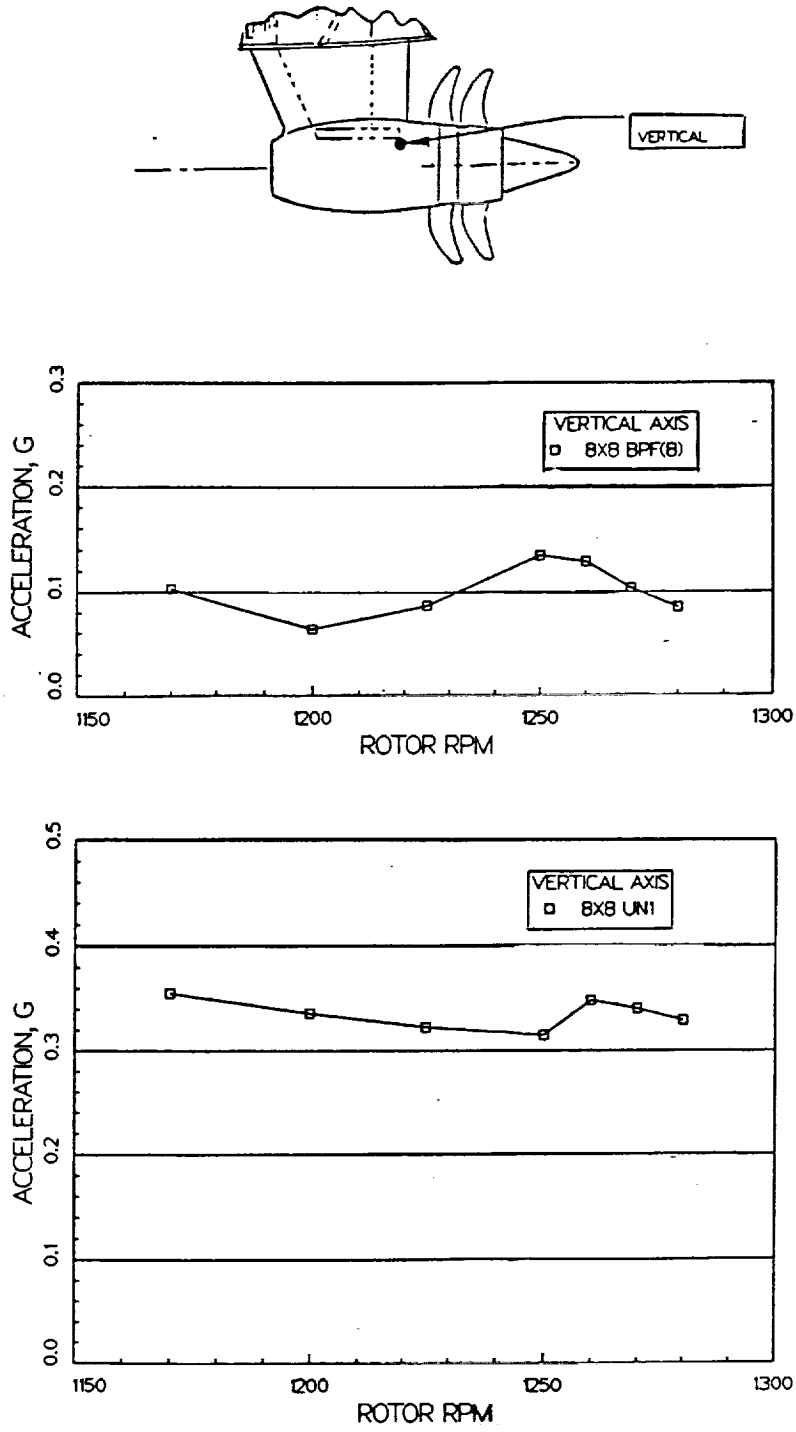

Figure 10: Aft Engine Mount Acceleration Levels - 8×8 UHB Engine

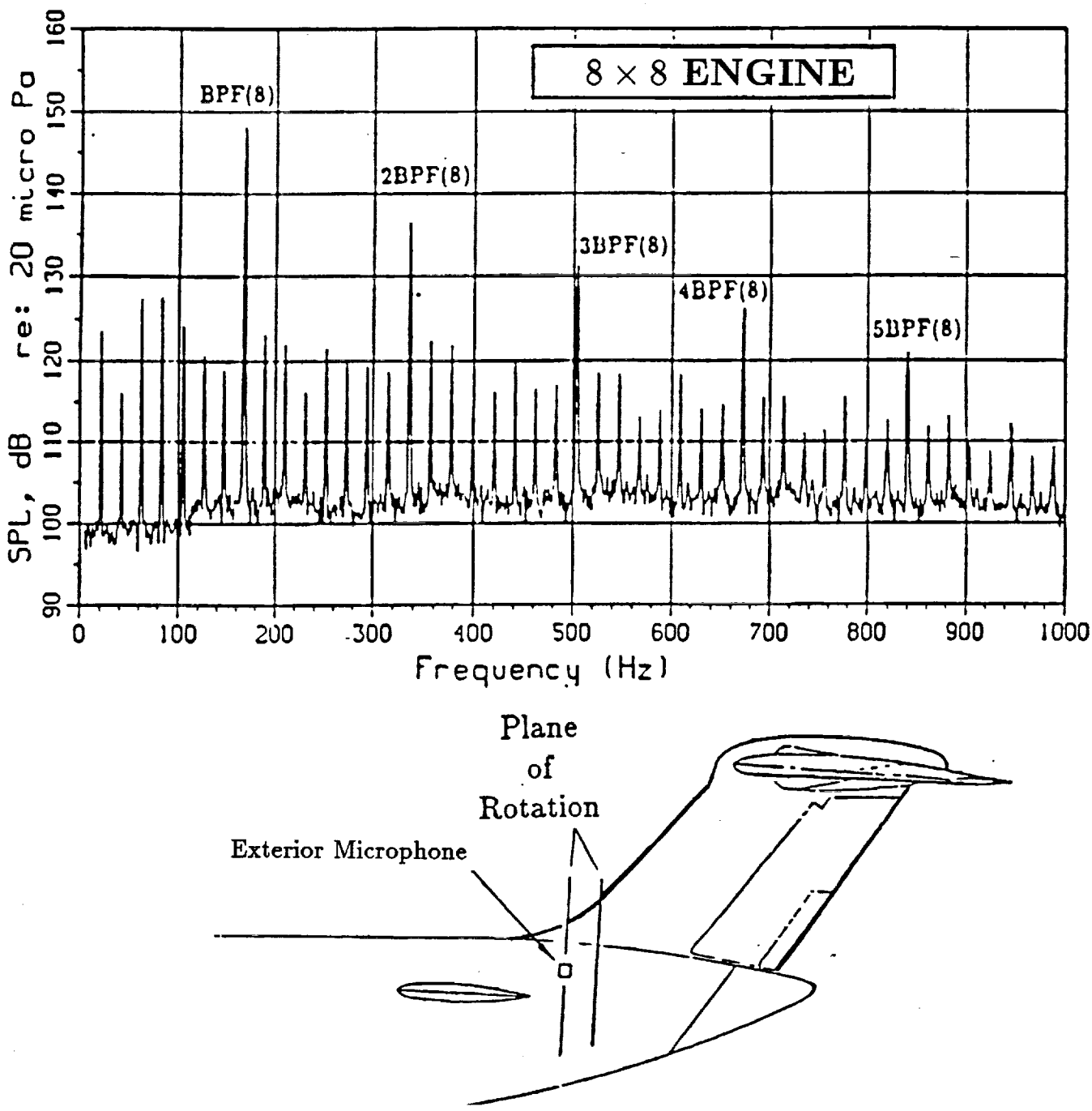

Figure 11: Exterior Noise Spectra on Aft Fuselage due to 8×8 UHB engine

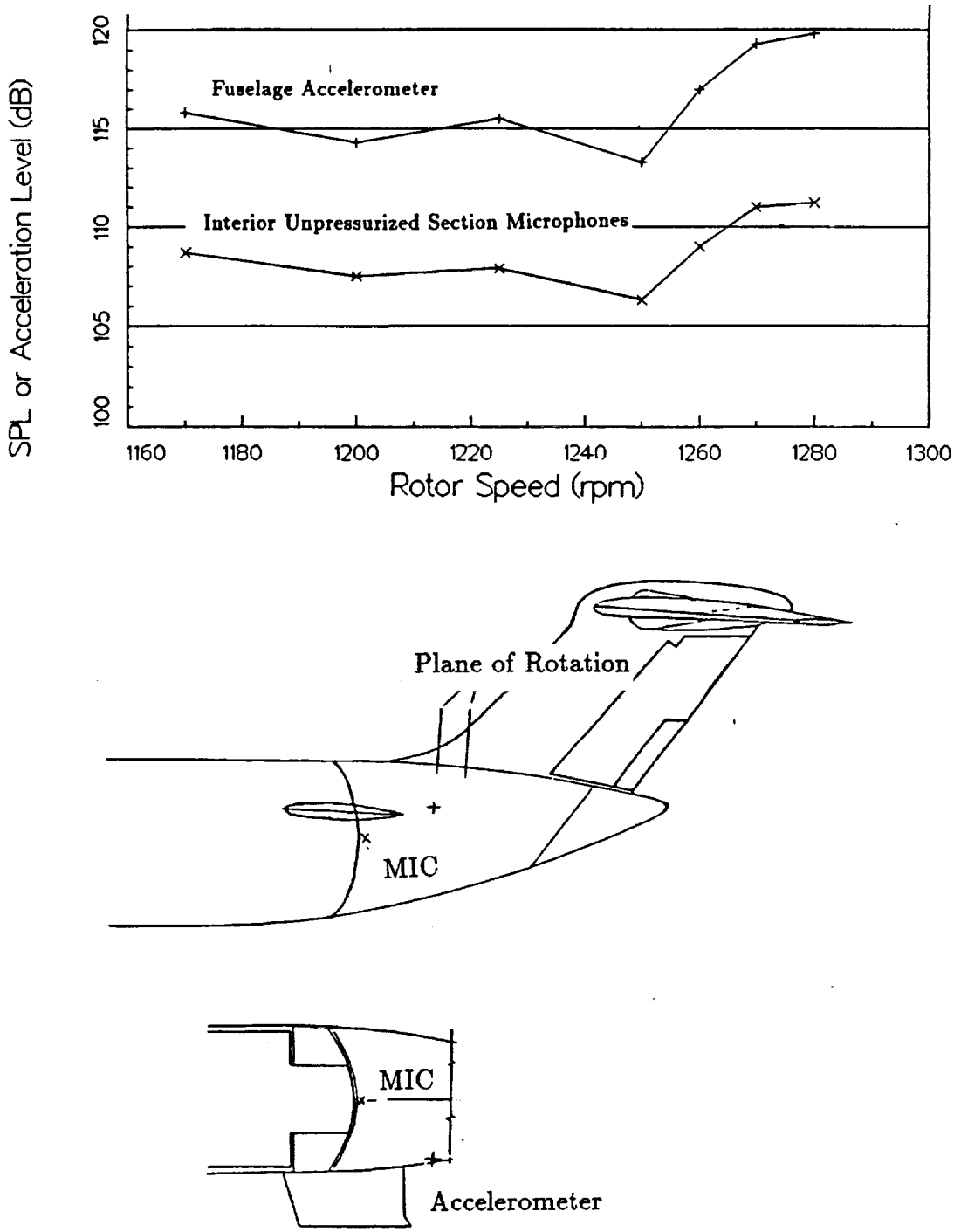

Figure 12: Aft Fuselage Section Vibration and Noise Levels due to 8×8 UHB engine

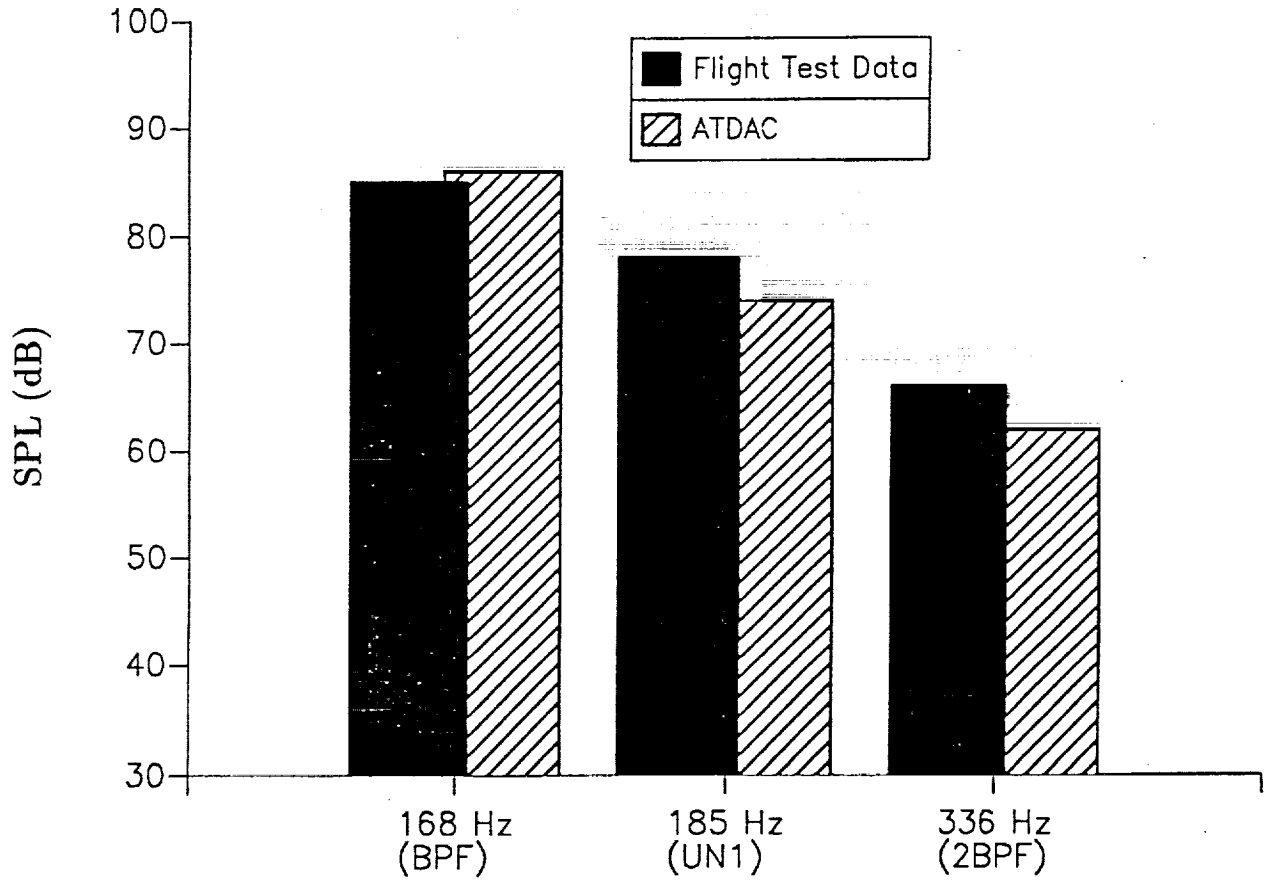

Figure 13: Comparison of ATDAC Predicted Airborne and Structure-Borne Cabin Noise Levels with Flight Test Data for MD-UHB Demonstrator Aircraft. (Altitude: 35000 ft, 0.76 Mach, 1260 RPM)

Sources: Boundary Layer + Airborne + Structure-Borne Tones
(Altitude: 35000 ft, Speed: 0.76 Mach, Propeller: 1260 RPM)

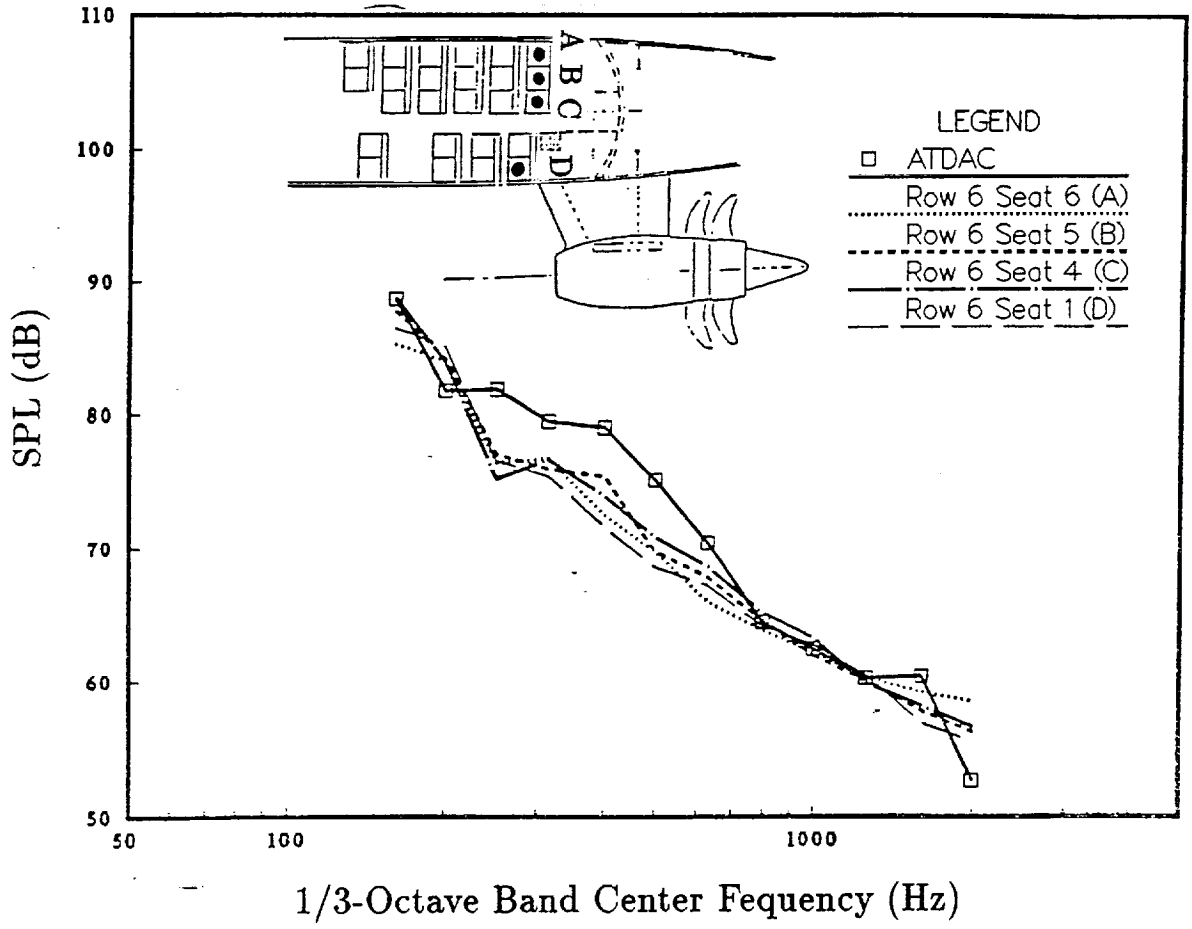

Figure 14: Comparison of ATDAC Predicted Cabin Noise Levels with Flight Test Data for MD-UHB Demonstrator Aircraft. (Altitude: 35000 ft, 0.76 Mach, 1260 RPM)

7 Conclusions

An analytical model for prediction of noise levels inside an aircraft cabin based on power balance, the acoustic room equation and transmission loss concepts has been developed. The theoretical basis for the computer program 'Acoustical Theory for Design of Aircraft Cabins (ATDAC)' is presented in this report. This program is a set of modules based on validated algorithms for prediction of turbulent boundary layer noise, transmission and reflection co-efficients of aircraft-type panels, structure-borne noise and interior noise levels. In ATDAC, these modules form a system to predict the aircraft interior noise levels from information about the acoustic sources, aircraft geometry and design. The details of the implementation of these algorithms are described in the following Report: "Interior Noise Prediction Methodology– ATDAC User's Manual." [1]

Flight and ground test interior noise and vibration data were used to validate the code's predictions. The predicted transmission loss for selected panel configurations were compared with laboratory test data. The boundary layer noise prediction model was validated using flight test data. The ATDAC predicted cabin noise components due to dominant airborne and structure-borne paths were compared with the measured data. The ATDAC interior noise prediction scheme was validated using flight test data for the MD-UHB Demonstrator aircraft. The ATDAC predicted cabin noise levels are in good agreement with the flight test data.

From the results presented in this report, it may be concluded that ATDAC provides a useful interior noise prediction methodology for aircraft cabins. A noise control designer can use the ATDAC program to compare the effects of different noise control treatments and thereby develop an aircraft configuration which meets interior noise criteria.

References

[1] Mathur, G. P., "Interior Noise Prediction Methodology: ATDAC User's Manual," Report prepared under NASA Contract NAS1-18037, 1992.

[2] Embleton, T.F.W., "Sound Pressure in Large Rooms," Chapter 9, *Noise and Vibration Control*, edited by L.L. Beranek, McGraw-Hill, New York (1971).

[3] Vér, I.L. and C.L. Holmer, "Interaction of Sound Waves with Solid Structures," Chapter 9, *Noise and Vibration Control*, edited by L.L. Beranek, McGraw-Hill, New York (1971).

[4] Fahy, F., *Sound and Structural Vibration*, Academic Press, London (1985).

[5] Hamada, Y. and H. Tachibana, "Analysis of Sound Transmission Loss of Multiple Structures by Four-Terminal Theory," *INTERNOISE 85 Proceedings*, Munich, 693-696 (1985).

[6] Bies, D. A., "Acoustical Properties of Porous Materials," Chapter 10, *Noise and Vibration Control*, edited by L.L. Beranek, McGraw-Hill, New York (1971).

[7] Grosveld, F. W. and J. S. Mixson,"Noise Transmission Through an Acoustically Treated and Honeycomb-Stiffened Aircraft Sidewall," *Journal of Aircraft*, **22** , No. 5, 434-440 (1985).

[8] Molloy, C. T., "Use of Four-Pole Parameters in Vibration Calculations," *Journal of the Acoustical Society of America*, **29** , No. 7, 842-853 (1957).

[9] Koval, L.R., "Effect of Air Flow, Panel Curvature, and Internal Pressurization of Field-incidence Transmission Loss," *Journal of the Acoustical Society of America*, **59** , No. 6, 1379-1385 (1976).

[10] Sharp, B.H., "A Study of Techniques to Increase the Sound Insulation of Building Elements," Wyle Laboratories Report WR 73-5, June 1973.

[11] Lyon, R.H., *Statistical Energy Analysis of Dynamic Systems: Theory and Applications*, MIT Press, Cambridge (1975).

[12] Lyon, R.H. and E. Eichler, "Random Vibrations of Connected Structures," *Journal of the Acoustical Society of America*, **36** , No. 7, 1344-1354 (1964).

[13] Swift, P.B., *The Vibrational Energy Transmission Through Connected Structures*, Ph.D. Thesis, University of Adelaide (1977).

[14] Maidanik, G., "Response of Ribbed Panels to Reverberant Acoustic Fields," *Journal of the Acoustical Society of America*, **34** , No. 6, 809-826 (1962).

[15] Lowson, M.V., "Prediction of Boundary Layer Pressure Fluctuations," AFFDL-TR-67-167, April 1968.

[16] Bies, D.W., "A Review of Flight and Wind Tunnel Measurements of Boundary Layer Pressure Fluctuations and Induced Structural Response," NASA CR 626, 1966.

[17] Bhat, W.V., "Flight Test Measurement of Exterior Turbulent Boundary Layer Pressure Fluctuations on Boeing Model 737 Airplane," *Journal of Sound and Vibration,* **14** No. 4, 439-457 (1971).

[18] Simpson, M.A. et al, "UHB Demonstrator Interior Noise Control Flight Tests and Analysis," NASA CR-181897, 1989.

REPORT DOCUMENTATION PAGE

Form Approved
OMB No. 0704-0188

1. AGENCY USE ONLY (Leave blank)	2. REPORT DATE	3. REPORT TYPE AND DATES COVERED
	April 1991	Contractor Report

4. TITLE AND SUBTITLE
Interior Noise Prediction Methodology: ATDAC Theory and Validation

5. FUNDING NUMBERS
C NAS1-18037
WU 535-03-11-03

6. AUTHOR(S)
Gopal P. Mathur and Bryce K. Gardner

7. PERFORMING ORGANIZATION NAME(S) AND ADDRESS(ES)
Douglas Aircraft Company
McDonnell Douglas Corporation
Long Beach, CA 90846

8. PERFORMING ORGANIZATION REPORT NUMBER

9. SPONSORING / MONITORING AGENCY NAME(S) AND ADDRESS(ES)
National Aeronautics and Space Administration
Langley Research Center
Hampton, VA 23665-5225

10. SPONSORING / MONITORING AGENCY REPORT NUMBER
NASA CR-187626

11. SUPPLEMENTARY NOTES
Langley Technical Monitor: Kevin P. Shepherd
Task 7 Assignment
Subtask 3 Report

12a. DISTRIBUTION / AVAILABILITY STATEMENT
Unclassified–Unlimited

Subject Category 71

12b. DISTRIBUTION CODE

13. ABSTRACT (Maximum 200 words)

The Acoustical Theory for Design of Aircraft Cabins (ATDAC) is a computer program developed to predict interior noise levels inside aircraft and to evaluate the effects of different aircraft configurations on the aircraft acoustical environment. The primary motivation for development of this program is the special interior noise problems associated with advanced turboprop (ATP) aircraft where there is a tonal, low frequency noise problem.

Prediction of interior noise levels requires knowledge of the energy sources, the transmission paths, and the relationship between the energy variable and the sound pressure level. The energy sources include engine noise, both airborne and structure-borne; turbulent boundary layer noise; and interior noise sources such as air conditioner noise and auxiliary power unit noise. Since propeller and engine noise prediction programs are widely available, they are not included in ATDAC. Airborne engine noise from any prediction or measurement may be input to this program. This report describes the theory and equations implemented in the ATDAC program.

14. SUBJECT TERMS	15. NUMBER OF PAGES
Acoustics; Aircraft Interior Noise; Noise Prediction; Noise Control; Advanced Turboprop Aircraft	50
	16. PRICE CODE

17. SECURITY CLASSIFICATION OF REPORT	18. SECURITY CLASSIFICATION OF THIS PAGE	19. SECURITY CLASSIFICATION OF ABSTRACT	20. LIMITATION OF ABSTRACT
Unclassified	Unclassified	Unclassified	Unlimited